Mon. Not. R. Astron. Soc. **279**, 1011–1018 (1996)

Infrared imaging of late-type stars

Željko Ivezić and Moshe Elitzur
Department of Physics and Astronomy, University of Kentucky, Lexington, KY 40506-0055, USA
e-mail: ivezic@pa.uky.edu, moshe@pa.uky.edu

Accepted 1995 November 23. Received 1995 November 23; in original form 1995 July 31

ABSTRACT
Infrared imaging properties of dusty winds around late-type stars are investigated in detail, employing a self-consistent model that couples the equations of motion and radiative transfer. Because of general scaling properties, the angular profiles of surface brightness are self-similar. In any given star, the profile shape is determined essentially by overall optical depth at each wavelength and it is self-similarly scaled by the size of the dust condensation zone. We find that the mid-IR is the best wavelength range to measure directly the angular size of this zone, and from *IRAS* data we identify the 15 best candidates for such future observations. We also show that the visibility function at short wavelengths ($\lesssim 2$ μm) directly determines the scattering optical depth, and produce theoretical visibility curves for various characteristic wavelengths and the entire parameter range relevant to late-type stars. The infrared emission should display time variability because of cyclical changes in overall optical depth, reflecting luminosity-induced movement of the dust condensation point. Calculations of the wavelength dependence of photometric amplitudes and time variability of envelope sizes are in agreement with observations; envelopes are bigger and bluer at maximum light.

Key words: circumstellar matter – stars: late-type – dust, extinction – infrared: stars.

1 INTRODUCTION

Ongoing progress in imaging techniques, expected to continue at an accelerated pace (e.g. Gezari & Backman 1993; Skinner et al. 1994), enables spatial resolution of infrared sources. The wealth of details provided by high-resolution data requires a commensurate theoretical effort, which can be expected in general to involve a large number of free parameters. The freedom afforded by many parameters usually produces good fits but casts doubt on the uniqueness of such models.

Late-type stars are a notable exception. Recently we have shown that, given the grain composition, the IR signature of dusty envelopes around such stars is essentially determined by a single parameter – the flux-averaged optical depth τ_F (Ivezić & Elitzur 1995; hereafter IE95). This parameter alone controls both the dynamics and IR emission. The fine resolution achieved in recent interferometric observations (envelopes are resolved on angular scales as small as 0.03 arcsec at ~ 10 μm; see Danchi et al. 1994) merits detailed modelling of these stars, which we offer here. The surface brightness distribution can be calculated once the density and temperature distributions of the dust in the envelope are known (e.g. Crabtree & Martin 1979). In previous studies, both distributions were usually modelled by power laws prescribed beforehand. Instead, here we determine these distributions self-consistently from a complete, detailed model that solves the envelope dynamics and radiative transfer simultaneously. This self-consistent approach enables us to compare different types of observations and to investigate systematically which techniques are best suited for determining various quantities.

General analysis of surface brightness distributions is described in Section 2. The effects of stellar variability on observed IR emission are discussed in Section 3. We analyse the observational implications of our results in Section 4 and summarize them in Section 5.

2 SURFACE BRIGHTNESS DISTRIBUTION

The surface brightness of a spherically symmetric source depends only on the impact parameter b, the displacement from the centre of symmetry. In the case of late-type stars, we have shown (IE95) that the solution of the radiative transfer problem is a self-similar function of the scaled variable b/r_1, where r_1 is the envelope's inner boundary, corresponding to the dust condensation radius. For a given type of dust grains, this function is virtually fully determined by the overall optical depth τ and does not depend separately on luminosity, mass-loss rate, etc.

Fig. 1 presents the results of our model calculations at the three representative wavelengths: 2.2, 5 and 10 μm. The surface brightness profile depends only on the dimensionless variable b/r_1, so that it scales self-similarly with the dust condensation radius r_1. At any given wavelength, the shape of this profile

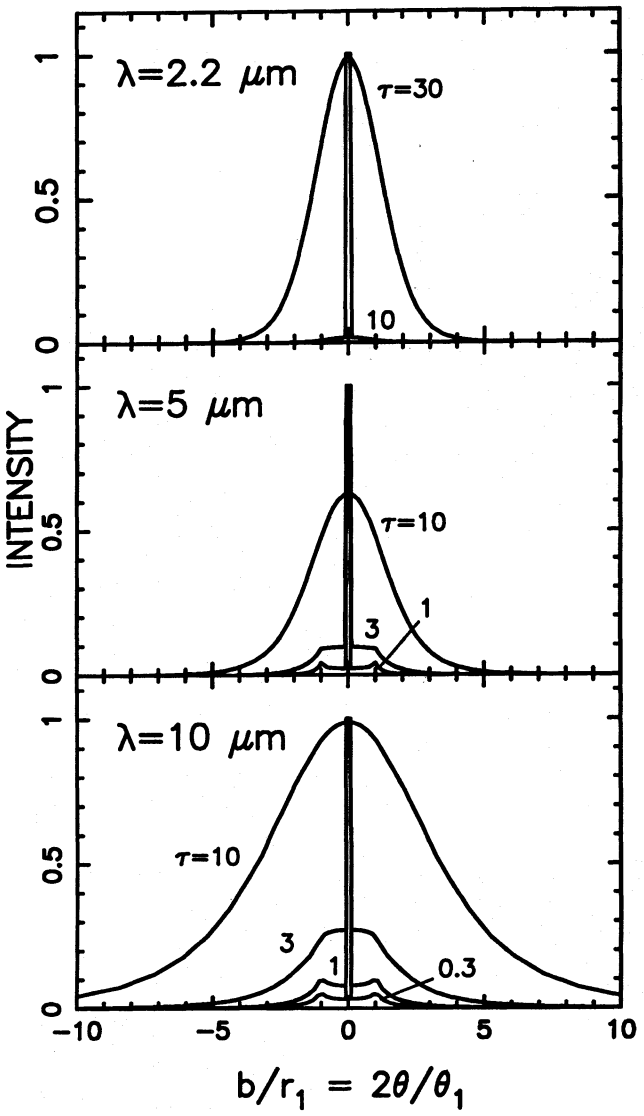

Figure 1. Normalized surface brightness distributions at 2.2, 5 and 10 μm for models with dust condensation temperature $T_1 = 800$ K, stellar temperature $T_* = 2500$ K and optical depths as marked. Here b and θ are, respectively, the linear and angular displacements from the centre, r_1 is the radius and θ_1 is the angular diameter of the dust condensation zone.

is determined by τ; two different systems with the same τ will have identical profiles in terms of b/r_1, so that the actual value of r_1 is irrelevant. For a system at distance D, the impact parameter b corresponds to an angular displacement $\theta = b/D$. If we introduce the angular diameter of the dust condensation zone $\theta_1 = 2r_1/D$, then the observed surface brightness is a self-similar function of $b/r_1 = 2\theta/\theta_1$.

In these calculations we have used a detailed model that takes into account the wind acceleration by radiation pressure, determined self-consistently from a solution of the coupled equations of hydrodynamics and radiative transfer (for details see Netzer & Elitzur 1993; IE95). Thanks to scaling, the displayed profiles are applicable to any late-type star at the optical depths indicated for each wavelength, with a given star corresponding to different optical depths at different wavelengths. The models were calculated with the opacities of amorphous carbon (Hanner 1988). Other types of grains (silicate, SiC, etc.) produce almost identical profiles for the same optical depths. For a given star, only the association of optical depths with wavelengths may depend on grain chemistry when there are spectral features in the opacity. For example, for the same optical depth at 2.2 μm, a star with silicate grains will have a larger 10-μm optical depth than one with carbon grains. Thus the two stars will have the same profile at 2.2 μm but different ones at 10 μm. The 10-μm profile will be the same for the star with silicate grains and another star with carbon grains whose τ is matched at that wavelength.

In addition to chemical composition, optical properties depend also on the grain size a. Except for spectral features, the absorption and scattering efficiencies are self-similar functions of the scaled variable $x = 2\pi a/\lambda$ and their functional form does not change when $x < 1$. Therefore, so long as only $x < 1$ is covered by observations, the grain size is largely irrelevant. For the wavelengths addressed here, $\lambda \geqslant 2.2$ μm, all grains smaller than ~ 0.2 μm are practically equivalent, and following IE95 we adopt a single grain size of 0.05 μm. The possible effect of grains larger then 0.2 μm is discussed below (Section 2.1). Other input parameters used in these calculations are the stellar temperature $T_* = 2500$ K and the dust condensation temperature $T_1 = 800$ K. The model results depend primarily only on the ratio of these two temperatures. Varying T_1 and T_* within their relevant ranges has a negligible effect on the results.

The narrow central component evident in the profiles is the stellar radiation attenuated by the dust shell. Its width is r_*/r_1, where r_* is the stellar radius. This ratio is directly related to T_*/T_1. The results of our detailed model calculations, which account for the contributions of both the central star and the dusty envelope to the radiation field at r_1, can be adequately summarized with

$$\frac{r_1}{r_*} = \alpha \left(\frac{T_*}{T_1}\right)^2. \qquad (1)$$

Here α is a dimensionless coefficient that depends primarily on the grains' optical properties and only weakly on the overall optical depth. For carbonaceous grains α is ~ 1.2 for $\tau = 0$, increasing slowly with τ to $\alpha \simeq 1.4$ at $\tau(2.2\ \mu\text{m}) \sim 50$, the largest plausible optical depth. For silicate grains, the corresponding range is ~ 0.5–0.8. In addition, α has an even weaker dependence on T_1 and T_*, which can be neglected in all practical applications.

The extended component visible in the figure is the contribution of the dust shell. At small τ this intensity component is proportional to the optical depth along the line of sight, and the displayed profiles reflect the behaviour of this function. The features evident at $b/r_1 = \pm 1$ simply reflect the envelope's inner edge. High-resolution imaging will delineate these features as a bright rim whose angular size (θ_1) is wavelength independent. The angular size of the dust formation zone is then directly measurable. In addition, the optical depth can be estimated by comparing the measured ratio of peak intensities of the central (stellar) component and the dust formation features with those of the displayed profiles. As the optical depth increases, these features gradually disappear and the shell's contribution approaches that of the star. The intensity profile becomes a featureless bell-shaped curve, whose width is roughly proportional to $\tau\theta_1$. In this case it is impossible to determine τ and θ_1 independently.

2.1 Visibility curves

Most spatially resolved IR observations of late-type stars are interferometric and produce the two-dimensional Fourier transform of the surface brightness, the visibility $V(q)$, where q is the spatial frequency. For a circularly symmetric intensity profile, $V(q) = F(q)/F(0)$, where

$$F(q) = 2\pi \int_0^\infty I(\theta) J_0(2\pi q\theta)\, \theta \mathrm{d}\theta \qquad (2)$$

(cf. Rogers & Martin 1984; J_0 is the Bessel function of zeroth order). In the present case

$$V(q) = f_S V_S + f_D V_D, \qquad (3)$$

where V_S and V_D are the individual visibility curves of the stellar and dust emission, respectively, and f_S and f_D are the fractional contributions of these two components to the total flux. The stellar component can be closely approximated by a uniform-brightness disc

$$V_S = \frac{2J_1(\pi q\theta_*)}{\pi q\theta_*}, \qquad (4)$$

where J_1 is the Bessel function of first order and $\theta_* = 2r_*/D$ is the angular diameter of the stellar disc. The stellar visibility is a function of $q\theta_*$. Because of scaling, the shell's contribution to the intensity is a self-similar function of θ/θ_1, thus the corresponding visibility V_D is a self-similar function of $q\theta_1$.

Fig. 2 presents the visibility curves of the surface brightness distributions displayed in Fig. 1, including more values of τ for optically thin envelopes. Just as the surface brightness profiles scale self-similarly with r_1, the visibility profiles scale self-similarly with θ_1. The dashed lines are the visibility curves of a naked star, V_S, included for comparison. They are quite flat, reaching zero visibility only at $q\theta_1 = 1.2\,\theta_1/\theta_* = 1.2\,r_1/r_*$. Note that the ratio r_1/r_*, typically $\sim$ 5–10, is directly related to the temperature ratio T_1/T_* (equation 1).

The stellar and envelope contributions are easily discernible in the figure. All visibility curves display an initial drop with $q\theta_1$, reflecting the extended nature of the dust component, followed by a levelling off when the envelope is fully resolved and the stellar component takes over. The value V_c of the visibility at that levelling-off is roughly the fraction of the stellar contribution to the total flux. The significance of this contribution depends on both optical depth and wavelength. When it is appreciable, V_c is finite and the levelling-off occurs at $q\theta_1 \sim 1$. The visibility curve can then be used to determine both θ_1 and τ – the magnitude of V_c directly gives τ, and the location of the levelling-off determines the angular scale $\theta_1 \simeq 1/q$. In sources where $V_c \simeq 0$, the levelling-off occurs at progressively smaller $q\theta_1$ as τ increases, a direct consequence of the broadening of the intensity profile (cf. Fig. 1). The visibility curves become self-similar with angular size-scale roughly proportional to $\tau\theta_1$, thus τ and θ_1 cannot be determined independently. These points have been recognized previously in the discussion of surface brightness.

It is important to note that the dust component of the visibility profiles always varies with wavelength, even in optically thin envelopes whose images are dominated by wavelength-independent bright rims (corresponding to the dust formation zone). The reason is that, at any given wavelength, the visibility reflects the angular size of the region from which most of the flux is emitted. This size corresponds to the radius where the dust temperature is comparable to the Wien temperature of that wavelength. Since the dust temperature decreases with distance, the size of the flux emitting region increases with wavelength. Such variation has been detected in many observations. Most visibility observations are interpreted in terms of Gaussian fits and are reported in terms of the resulting Gaussian FWHM θ_G. A quantitative comparison of theory with observations must incorporate this widespread method of reporting observational results. The observed Gaussian widths are found to increase with wavelength according to $\theta_G \propto \lambda^k$, and the index k is found to vary considerably among individual stars. In the wavelength range 2–10 μm, Dyck et al. (1984) obtained $k \sim 0.2$ for C stars (carbon dust) and $k \sim 0.7$–1.3 for O stars (silicate dust). Cobb & Fix (1987) found $k \sim 1$ in the wave-

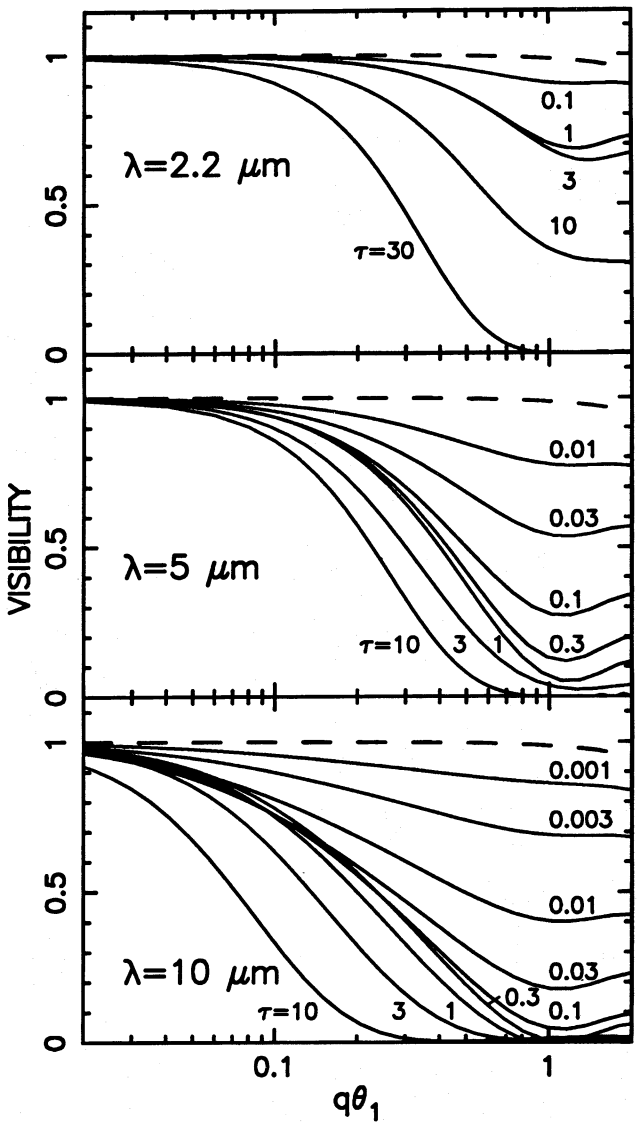

Figure 2. Visibility curves (q is the spatial frequency) at 2.2, 5 and 10 μm for models with the same temperatures as in Fig. 1 and optical depths as marked. The dashed line is the visibility function of the naked star ($\tau = 0$).

length range 5–10 μm for a sample of OH/IR stars (silicate dust).

Our models readily explain these detailed observations. Fitting a Gaussian to the model visibilities, we find that in the wavelength range 2.2–10 μm these fits can be summarized with

$$\theta_G \simeq \theta_1 \left(\frac{\lambda}{3.2\,\mu\mathrm{m}}\right)^{0.6} \times \begin{cases} 1 & \tau \leqslant 1 \\ \tau^{0.4} & \tau > 1, \end{cases} \quad (5)$$

an approximation accurate to within 10–20 per cent. Therefore, in optically thin envelopes $k = 0.6$ independent of grain chemical composition, in agreement with the lower bound of the range found in O stars by Dyck et al. In optically thick envelopes, on the other hand, k does vary with the grain chemistry because of its dependence on τ. We find that $\theta_G \propto \lambda^{0.2}$ in amorphous carbon optically thick envelopes, in agreement with the observations of C stars. The results for silicate grain optically thick envelopes are more involved because of the peak at 9.7 μm. A parametrization in the form $\theta_G \propto \lambda^k$ results in $k = 1.3$ when the fit applies to the wavelength range 2–10 μm and $k = 4$ for the range 7–10 μm. These results are in agreement with the various O star observations quoted above.

In addition, observations by Fix & Cobb (1988) at 8 and 10 μm show that θ_G is roughly the same at both wavelengths in IRC+10420 but increases by about a factor of 2.5 in OH 26.5+0.6, even though both stars display the silicate feature. Our results explain both observations if the dust shell is optically thin in IRC+10420 (expected θ_G variation of only 10 per cent) and thick in OH 26.5+0.6 (expected variation by a factor of 2.4). Indeed, the former displays the silicate feature in emission, the latter in absorption, indicating optically thin and thick envelopes, respectively.

In spite of these successes, our model results indicate that single-Gaussian fits to visibility curves must be used with great care. Such fits are adequate within observational uncertainties (~ 0.05 in visibility) only at short wavelengths ($\lesssim$ 2.2 μm). The quality of Gaussian fitting deteriorates as the wavelength increases, and we find such fitting meaningless for $\lambda \gtrsim 10$ μm. The apparent success of Gaussian fits at such wavelengths in a number of actual observations usually reflects partial coverage of the visibility curve (e.g. Sutton, Betz & Storey 1979, $V \leqslant 0.5$; Cobb & Fix 1987, $V \geqslant 0.8$). Indeed, when the spatial frequency coverage provides the entire visibility curve, single-Gaussian fits become inadequate (e.g. Mariotti et al. 1983; Dyck et al. 1987). While such a fitting procedure fails, our models provide satisfactory fits to all observations and provide a more adequate method for data analysis.

Finally, for given a grain size a, scattering is important only for wavelengths shorter than $\lambda_{sca} = 2\pi a$. For the size used here of 0.05 μm, λ_{sca} is 0.3 μm and scattering is negligible at all the displayed wavelengths. For any plausible grain size ($\lesssim$ 1 μm), scattering can become important only at the shortest displayed wavelength of 2.2 μm. When that happens, the shape of the visibility curves remains essentially the same but the corresponding optical depth is significantly smaller. For example, if the grain size is 0.2 μm, the five curves in the topmost panel of Fig. 2 are produced with optical depths of 0.1, 0.8, 1, 3 and 10, respectively, instead of the indicated values of 0.1, 1, 3, 10 and 30.

3 TIME VARIABILITY

Late-type stars display variability with periods of order years and bolometric amplitudes of 1–2 mag (e.g., Blommaert 1992). The bolometric luminosity variability affects the infrared properties through changes of the dust condensation radius and overall optical depth. Combining equation (1) with the luminosity relation $L_* = 4\pi r_*^2 \sigma T_*^4$ produces

$$r_1 = 2.3 \times 10^{14} \alpha \left(\frac{L_*}{10^4\ \mathrm{L}_\odot}\right)^{1/2} \left(\frac{10^3\ \mathrm{K}}{T_1}\right)^2 \mathrm{cm}. \quad (6)$$

A similar relation for galactic nuclei was noted in the recent numerical work of Laor & Draine (1993). Luminosity variability induces movement of the dust condensation point: the shell's inner boundary is furthest from the star at maximum light. This variation in linear scale-size of the envelope translates directly to its angular scale size, θ_1. *Envelopes are larger during maximum luminosity.* It is noteworthy that variations of stellar radius and temperature during the stellar cycle do not enter independently, only through the overall luminosity.

Such dependence of envelope size on phase of the light curve has been detected. McCarthy, Howell & Low (1978) found that Mira (*o* Ceti) was partially resolved at 10.2 μm near maximum visual phase but unresolved at minimum phase. McCarthy, Howell & Low (1980) measured the size of IRC+10216 at 5 μm and obtained a larger value at maximum than at minimum of the light curve. Danchi et al. (1990, 1994) reobserved this source at 11 μm and confirmed these results. In a separate study (Ivezić & Elitzur 1996; hereafter IE96) we analyse in detail all observations of IRC+10216 and show that the angular diameter of its dust condensation zone varies between ~ 0.3 and ~ 0.5 arcsec as the luminosity changes from minimum to maximum.

Variations of r_1 during the stellar cycle affect the dust optical depth so that τ should be smallest at maximum light, largest at minimum. If the grain optical properties do not change during the stellar cycle, the overall optical depth is proportional to the dust column density. For constant mass-loss rate $\dot{M}$ and velocity v_1 at the base of the envelope, the dust column density scales with r_1^{-1}. Together with equation (6), this implies $\tau \propto L_*^{-1/2}$. Since both $\dot{M}$ and v_1 may vary during the stellar cycle, the dependence of τ on L_* can be expected to be somewhat different but still show the same trend. From detailed analysis we find that, in IRC+10216, $\tau \propto L_*^{-0.2}$ (IE96). Because of the variation of τ, IR spectral properties should vary with the light curve, corresponding to redder radiation at minimum light (largest optical depth), bluer at maximum. Indeed, ever since the work of Pettit & Nicholson (1933), such behaviour has manifested itself in many observational correlations. In particular, Le Bertre (1988a,b) finds that in several dusty envelopes the wavelength of peak emission is shorter at maximum than at minimum light. In general, *envelopes are bluer around maximum light.*

The phase dependence of optical depth can be analysed quantitatively with the aid of photometric amplitudes $A = 2.5 \log(F^{max}/F^{min})$, where F^{max} and F^{min} are fluxes at maximum and minimum light, respectively. At each wavelength, the photometric amplitude A_λ is related to the amplitude A_{bol} of the bolometric flux F via

$$A_\lambda = A_{bol} + a_\lambda, \quad (7)$$

where a_λ is the amplitude of normalized flux $f_\lambda = F_\lambda/F$. Because of scaling, f_λ does not depend separately on luminosity, mass-loss rate, etc., only on overall optical depth (IE95). Therefore, a_λ is a unique function of τ, specifically

$$a_\lambda(\tau) = 2.5 \log \frac{f_\lambda(\tau^{\max})}{f_\lambda(\tau^{\min})}, \tag{8}$$

where $\tau^{\max}$ and $\tau^{\min}$ are the optical depths at maximum and minimum light, respectively. That is, for a given dust chemical composition, a_λ too does not depend on individual properties other than optical depth. Our detailed model calculations show that a_λ has a simple behaviour in two distinct limits. At wavelengths for which $\tau < 1$, typically $\lambda \gtrsim 20$ μm, $a_\lambda \propto -A_{\rm bol}$. At wavelengths for which emission can be neglected, typically $\lambda \lesssim 3$ μm (wavelengths shorter than the peak of the Planck function of the dust formation temperature T_1), $a_\lambda \propto \tau_\lambda$. From these results we find that

$$A_\lambda \simeq \begin{cases} A_{\rm bol} + 0.7\tau_\lambda & \lambda \lesssim 3\ \mu\text{m} \\ (0.5 - 0.7) \times A_{\rm bol} & \lambda \gtrsim 20\ \mu\text{m}. \end{cases} \tag{9}$$

The photometric amplitudes vary linearly with τ in the near-IR, becoming wavelength independent in the mid- and far-IR. Since $A_{\rm bol}$ varies little among stars while τ varies a lot, the range of photometric amplitudes can be expected to be large at short wavelengths, small at long ones. In addition, τ decreases with wavelength in the near-IR, thus the amplitudes should decrease too.

These simple results readily explain the available observations. Short-wavelength amplitudes indeed decrease with wavelength and visual amplitudes are usually much larger than bolometric ones (e.g. Hetzler 1936; Lockwood & Wing 1971). Furthermore, analysis of the Harvey et al. (1974) observations shows that near-IR amplitudes of different stars increase with overall optical depth, and for a given star decrease with wavelength. This behaviour is confirmed by subsequent observations (e.g. DiGiacomo et al. 1991). Finally, the spread among stars is much larger for visual than for bolometric amplitudes (e.g. Forrest, Gillet & Stein 1975). For long wavelengths, Herman et al. (1984) find that the variation of OH maser luminosity, and presumably far-IR flux at 35 μm, is about half that of the bolometric luminosity.

Dust spectral features can display a more complex variability with the stellar phase. Depending on initial optical depth, the strength of the 9.7-μm silicate emission feature can either increase or decrease for the same change of τ: in optically thin envelopes the strength increases with τ until it reaches maximum at some optical depth $\tau_{\rm m}$ (~ 1), after which it decreases because of self-absorption (IE95). As a result, in envelopes with $\tau < \tau_{\rm m}$ the 9.7-μm emission feature is strongest during minimum light (the optical depth is largest), with the reverse behaviour in envelopes with $\tau > \tau_{\rm m}$. In envelopes with $\tau \sim \tau_{\rm m}$, the emission feature can remain almost unchanged during the stellar cycle. Little-Marenin, Staley & Stencel (1993) find examples for each type of behaviour in a number of sources that display the 9.7-μm emission feature. On the other hand, when this feature is in absorption, its depth always increases with τ (Scoville & Kwan 1976; IE95). Thus it is always deepest at minimum light, as observed (e.g. Engels et al. 1983).

4 OBSERVATIONAL IMPLICATIONS

The source intensity is a unique function of various intrinsic properties such as luminosity, mass-loss rate, dust density, dust-to-gas ratio, etc. However, because of scaling, intrinsic properties do not enter separately, only indirectly through their effect in determining τ and r_1. For given grain optical properties, the surface brightness is a unique function of the scaled variable b/r_1, essentially determined by overall optical depth. Since optical depths involve only intrinsic properties, the same applies to the self-similar profiles displayed in Figs 1 and 2. Contact with observations brings in the distance to the source, which fixes the scales of angular size θ_1 and bolometric flux F; that is, the distance sets the scale of conversion from linear to angular sizes and from intrinsic to observed fluxes. An additional dependence on the intrinsic parameters T_1 and T_* does exist, but it is rather weak and affects only optically thin envelopes at short ($\lesssim 7$ μm) wavelengths. Furthermore, compared with the variation range of τ and θ_1, T_1 and T_* are practically constant among late-type stars. As a result, the only non-radiative system properties that generally can be determined by the most detailed IR observations are τ (including its wavelength dependence), a purely intrinsic property, and θ_1, which sets the scales for observations. We discuss now which observational techniques are most suitable for determining these two quantities.

The least detailed observations are unresolved flux measurements, determining the spectral energy distribution F_λ. This function is the product of the spectral shape f_λ and the bolometric flux F. For given grains, the intrinsic property f_λ is controlled by τ and is independent of θ_1, thus it cannot be used to determine θ_1. However, for this very reason – its dependence on a single quantity – spectral shape analysis is the most reliable method for determining τ and its wavelength dependence, resulting in the best handle on the dust chemical composition. The additional information contained in the bolometric flux allows an estimate of θ_1, described below, albeit an indirect one.

Direct determination of θ_1 requires spatially resolved observations. However, as shown in Section 2, θ_1 and τ enter independently only in optically thin envelopes. In such sources, θ_1 can be directly read off the radial profiles from the position of the dust features, and τ determined from the intensity ratio of stellar and dust components (cf. Fig. 1). This determination of τ is considerably less certain than that of θ_1. As a result, the surface brightness distribution is always a poor indicator of τ, suggesting that the most practical approach involves a two-step data analysis procedure. In the first step τ is determined from a fit to the spectral shape, and in the second the resulting model prediction for the surface brightness is used to determine θ_1. We have used such a two-step approach to analyse the IR observations of IRC+10216, and with a single model obtained successful fits to all spectral and spatially resolved observations (IE96).

We proceed now to a more detailed discussion of the capabilities of different high-resolution techniques.

4.1 Direct imaging

Direct imaging is the best method for determining θ_1, from the location of the features corresponding to dust condensation. Unfortunately, these features are visible only for a limited

range of optical depths. At large τ the features are smeared out as the profile evolves into a bell shape. At small values of τ, the features are so weak compared with the stellar component that they become undetectable at the dynamic range of most current telescopes; note, however, that on telescopes such as *HST*, Keck or Gemini, a dynamic range of 1000 is possible in images at spatial resolutions better than 0.1 arcsec. As a result, at every wavelength the features are a useful indicator only when the optical depth is of order unity. Thus the features generally cannot be used at either end of the spectrum: at short wavelengths ($\lesssim$ 2–3 μm), the dust contribution is minute in comparison with the stellar component when $\tau \sim 1$ so the features are hard to resolve; and, at long wavelengths ($\gtrsim$ 20–30 μm), τ never reaches unity for the majority of late-type stars (IE95). Therefore, *the mid-infrared is the best spectral range for resolving the dust condensation features in surface brightness profiles.*

Table 1 lists the late-type stars we have identified as the best candidates for observations that can potentially resolve the dust formation features. They were selected as the stars with the largest expected values of θ_1 among *IRAS* sources whose 10 μm optical depth is in the range 0.1–2. In searching the *IRAS* catalogue we were careful to include only sources with the highest flux qualities in all four wavebands and uncontaminated by cirrus emission (see IE95 for details of the selection process and removal of contaminated sources). The optical depth was determined from the *IRAS* fluxes through extensions of the techniques of IE95, described in the Appendix. Estimating the angular size θ_1 is more involved. Our starting point is the relation

$$\theta_1 = 0.17\,\alpha \left(\frac{F}{10^{-8}\,\mathrm{W\,m^{-2}}}\right)^{0.5} \left(\frac{10^3\,\mathrm{K}}{T_1}\right)^2 \text{ arcsec}, \qquad (10)$$

obtained by combining equation (6) with $L_* = 4\pi D^2 F$; note that, when θ_1 and F are directly measured in observations, this equation can be inverted to determine the dust condensation temperature T_1. The Appendix describes a method for estimating the bolometric flux F from the *IRAS* fluxes, and for simplicity we assume $T_1 = 800$ K for all stars. The resulting estimates for θ_1 are expected to be accurate to within a factor of 2 or so. Table 1 presents the five sources with the largest θ_1 that we identified in each of the following LRS classes: 10 (featureless spectra), 20 (silicate 9.7-μm feature in emission) and 40 (11.3-μm in emission, mixture of amorphous carbon and SiC grains).

4.2 Visibility observations

All the radiative information available is contained in the surface brightness distribution. Therefore, direct imaging would be in principle the ultimate method to determine the system properties. However, finite dynamical range limitations preclude direct imaging of systems with very thin envelopes, where the intensity of dust emission is negligible in comparison with the stellar component. The structure of such systems can still be probed by visibility observations for the following reason. As is evident from equation (2), visibility is a measure of flux rather than intensity. Also, because of the much larger area of the dust emission, its flux can exceed that of the star even when the relation between intensities is the reverse.*

At wavelengths shorter than $\sim$ 2 μm and albedo $\gtrsim$ 0.1, the emission component of the dust radiation field is much weaker than either the scattered component or the direct stellar contribution because it requires dust warmer than plausible condensation temperatures. The radiation field is mostly composed of the attenuated stellar component and scattered light, and we find from our detailed solutions that under these circumstances

$$V_c \simeq \exp(-\tau_{sca}), \qquad (11)$$

where τ_{sca} is the scattering optical depth. This relation has a simple physical explanation and it is valid for $\tau_{sca} \lesssim 2$. With this relation, visibility observations can determine the wavelength dependence of τ_{sca}, a variation that can then be used to estimate the grain size a. The scattering optical depth is constant at short wavelengths, changing its behaviour to $\tau_{sca} \propto \lambda^{-4}$ for $\lambda \gtrsim \lambda_{sca} = 2\pi a$. Determining λ_{sca} from the change in behaviour of τ_{sca} yields an estimate for a. We have applied this method to the visibility observations of IRC+10216 and obtained $a \sim 0.2$ μm, in agreement with an independent estimate based on spectral shape analysis (IE96).

5 DISCUSSION

As shown in our previous study (IE95), the dynamics and spectral energy distributions of dusty winds around late-type stars are controlled by the dust chemical composition and overall optical depth. Here we have shown that a complete description of observations requires one additional parameter – the angular size of the dust condensation zone. Since the spectral shape is entirely independent of θ_1 it is the most reliable indicator of τ, whereas spatially resolved observations provide the most useful measurement of the dust condensation zone. Thus the most practical method of analysis is to determine the optical depth from model fits to the spectral shape, and θ_1 from high-resolution observations (either direct imaging or visibility). Because of scaling, the model results presented here and in IE95 provide sufficient coverage of parameter space for the analysis of virtually any late-type star. An example of such complete analysis is presented in IE96 for IRC+10216.

Our models do not include the effects of light travel time between the central star and the heated dust. The phase lags that such travel introduces between variations of the dust and stellar components are insignificant at short- and mid-infrared wavelengths, whose emission originates close to the dust condensation zone. At long wavelengths, however, the dust emission originates sufficiently far from the star that the phase lags can become appreciable. Analysis of this effect has been recently reported by Wright & Baganoff (1995), who show that it can be used to determine the distance to the star. It is important to note that these effects do not invalidate our steady-state modelling, as discussed in IE95.

In optically thin envelopes, our model images have a bright rim at the dust condensation radius, leading to the only

* This also implies that the stellar component can dominate the intensity profile even when it is negligible in the visibility observations. This is contrary to a conclusion by Griffin (1990).

Table 1. Best candidates for imaging: late-type stars identified from their *IRAS* fluxes as the most promising candidates for potential resolution of the dust condensation zone in future observations. Quantities tabulated in columns (d)–(f) are model-based estimates.

IRAS Name	Other Name[a]	LRS[b]	F_{12}[c]	τ_F[d]	τ_{10}[e]	θ_1[f]
05027−2158	T Lep	15	157	1.36	0.23	0.03
11294−6257	na	15	5	3.95	1.76	0.05
12380+5607	Y UMa	15	193	0.89	0.15	0.04
17297+1747	V833 Her	14	559	2.24	0.38	0.05
20120−4433	RZ Sgr	16	38	1.91	0.32	0.02
03507+1115	IK Tau	26	4630	0.12	0.39	0.22
04566+5606	TX Cam	27	1640	0.05	0.17	0.22
07209−2540	VY CMa	24	9920	0.27	0.87	0.31
18050−2213	VX Sgr	26	2740	0.11	0.37	0.20
23558+5106	R Cas	24	1340	0.06	0.20	0.17
09116−2439	na	42	737	1.43	0.22	0.07
15082−4808	na	42	793	1.41	0.21	0.08
17049−2440	na	42	793	1.79	0.27	0.08
18240+2326	na	42	731	1.73	0.26	0.07
23320+4316	LP And	42	959	1.09	0.16	0.09

(a) na: *IRAS* source without known association. (b) *IRAS* LRS class. (c) *IRAS* flux at 12 μm (Jy). (d) Flux-averaged optical depth. (e) Optical depth at 10 μm. (f) Angular size of the dust condensation zone (arcsec).

features, except for the stellar spike, in the surface brightness distribution. Images of optically thick envelopes do not display any details. We did not consider here the interaction of the wind with the surrounding interstellar medium, which may produce a dense shell far from the star (IE95). Such a shell would produce additional features in the surface brightness profile at long wavelengths ($\gtrsim$ 50 μm), which may have been observed for some *IRAS* stars at 60 and 100 μm (Young, Phillips & Knapp 1993). Indeed, from the observed angular sizes of these features Young et al. conclude that they probably correspond to the interface of the wind and the interstellar medium.

ACKNOWLEDGMENTS

This research has made use of the SIMBAD database, operated at CDS, Strasbourg, France, and the ADS database. Support by NSF grant AST-9321847, NASA grant NAG 5-3010 and the centre for Computational Sciences of the University of Kentucky is gratefully acknowledged.

REFERENCES

Blommaert J., 1992, PhD thesis, Sterrewacht Leiden
Cobb M.L., Fix J.D., 1987, ApJ, 315, 325
Crabtree D.R., Martin P.G., 1979, ApJ, 227, 900
Danchi W.C., Bester M., Degiacomi C.G., McCullough P.R., Townes C.H., 1990, ApJ, 359, L59
Danchi W.C., Bester M., Degiacomi C.G., Greenhill L.J., Townes C.H., 1994, AJ, 107(4), 1469
DiGiacomo A., Richichi A., Lisi F., Calamai G., 1991, A&A, 249, 397
Dyck H.M., Zuckerman B., Leinert Ch., Beckwith S., 1984, ApJ, 287, 801
Dyck H.M., Zuckerman B., Howell R.R., Beckwith S., 1987, PASP, 99, 99
Engels D., Kreysa E., Schultz G.V., Sherwood W.A., 1983, A&A, 124, 123
Fix J.D., Cobb M.L., 1988, ApJ, 329, 290
Forrest W.J., Gillet F.C., Stein W.A., 1975, ApJ, 195, 423
Gezari D.Y., Backman D.E., 1993, in McLean I., ed., Astronomy with Infrared Arrays – The Next Generation. Kluwer, Dordrecht, p. 57
Griffin I.P., 1990, MNRAS, 247, 591
Hanner M.S., 1988, Infrared Observations of Comets Halley and Wilson and Properties of the Grains. NASA89-13330, p. 22
Harvey P.M., Bechis K.P., Wilson W.J., Ball J.A., 1974, ApJS, 27, 331
Herman J., Isaacman R., Sargent A., Habing H., 1984, A&A, 139, 171
Hetzler C., 1936, ApJ, 83, 372
Ivezić Ž., Elitzur M., 1995, ApJ, 445, 415 (IE95)
Ivezić Ž., Elitzur M., 1996, MNRAS, 279, 1019 (IE96, this issue)
Laor A., Draine B.T., 1993, ApJ, 402, 441
Le Bertre T., 1988a, A&A, 190, 79
Le Bertre T., 1988b, A&A, 203, 85
Little-Marenin I.R., Staley S.B., Stencel R.E., 1993, in Kwok S., ed., ASP Conf. Ser. Vol. 41, Astronomical Infrared Spectroscopy: Future Observational Directions. Astron. Soc. Pac., San Francisco, p. 117
Lockwood G.W., Wing R.F., 1971, ApJ, 169, 63
Mariotti M., Chelli A., Foy R., Léna P., Sibille F., Tchountov G., 1983, A&A, 120, 237
McCarthy D.W., Howell R., Low F.J., 1978, ApJ, 223, L113
McCarthy D.W., Howell R., Low F.J., 1980, ApJ, 235, L27
Netzer N., Elitzur M., 1993, ApJ, 410, 701
Pettit E., Nicholson S.B., 1933, ApJ, 78, 320
Rogers C., Martin P.G., 1984, ApJ, 284, 327
Scoville N.Z., Kwan J., 1976, ApJ, 206, 718
Skinner C.J., Meixner M.M., Hawkins G.W., Keto E., Jernigan J.G., Arens J.F., 1994, ApJ, 423, L135
Sutton E.C., Betz A.L., Storey J.W.V., 1979, ApJ, 230, L105
Wright E.L., Baganoff F.K., 1995, ApJ, 440, 322
Young K., Phillip T.G., Knapp G.R., 1993, ApJ, 409, 725

APPENDIX A: OPTICAL DEPTHS AND BOLOMETRIC FLUX FROM *IRAS* DATA

Dust emission from late-type stars with envelopes is controlled by a single parameter, the flux averaged optical depth τ_F. The dependence of various spectral quantities on τ_F is listed by IE95, who also describe a method for determining τ_F from *IRAS* fluxes. Here we provide some additional useful relations, derived from our full model calculations.

Once τ_F is known, the optical depth at any wavelength can be obtained from

$$\tau_\lambda = t_\lambda \tau_F^n. \tag{A1}$$

The power n is 1 for all dust grains when $\tau_F \leqslant 1$. When $\tau_F > 1$, n is 0.5 for silicate-based grains and 1.7 for carbonaceous grains. The constants t_λ at selected wavelengths are listed in Table A1 for various grain compositions. For other wavelengths, t_λ can be interpolated using fig. 1 of IE95. Extrapolation toward shorter wavelengths is risky because of the increased contribution of scattering.

An additional useful correlation involves the bolometric flux and *IRAS* fluxes:

$$F = C \times 10^{-12} F_{60} \left(\frac{F_{12}}{F_{25}}\right)^\gamma \quad \mathrm{W\,m^{-2}}. \tag{A2}$$

Table A1. Constants for equation (A1).

λ (μm)	Sil.[a]	Oli.[b]	am.C[c]	SiC[d]
2.2	0.4	0.4	1.20	1.10
10.0	3.2	3.6	0.17	0.15
12.0	1.5	1.9	0.12	0.18
25.0	1.2	1.5	0.05	0.04
60.0	0.2	0.2	0.01	0.01

(a) Astronomical silicate. (b) Mixture of 80 per cent (by mass) astronomical silicate and 20 per cent crystalline olivine. (c) Amorphous carbon. (d) Mixture of 80 per cent (by mass) amorphous carbon and 20 per cent SiC.

Here F_{12}, F_{25} and F_{60} are *IRAS* fluxes in Jy, and C and γ are constants that depend on the dust chemical composition. For silicate-based grains $C = 7$ and $\gamma = 3$. For carbonaceous grains $C = 0.08$ and $\gamma = 6$ when $F_{12} > 2F_{25}$ and $C = 1.8$, $\gamma = 1.5$ otherwise.

This paper has been produced using the Royal Astronomical Society/Blackwell Science LaTeX style file.